The QUAX R&D at LNF

D. Alesini, D. Babusci, G. Ceccarelli (Tecn.), D. Di Gioacchino, C. Gatti (Resp.)
G. Lamanna (UniPI), C. Ligi, G. Maccarrone, D. Moricciani, G. Papalino(Tecn.), G. Pileggi (Tecn.)
A. Rettaroli (Dott.), F. Tabacchioni (Tecn. INAF), S. Tocci (Bors.)

1 Operation of a ferromagnetic Axion haloscope at $m_a = 58\,\mu$eV

In the QUAX experiment, dark matter axions are searched by means of their resonant interactions with electronic spins in a magnetized sample. In principle, axion-induced magnetization changes can be detected by embedding a sample in an rf cavity in a static magnetic field. In a recent work [1)] we described the operation of a prototype ferromagnetic haloscope, with a sensitivity limited by thermal fluctuations and receiver noise. With a preliminary dark matter search, we were able to set an upper limit on the coupling constant of DFSZ axions to electrons $g_{aee} < 4.9 \times 10^{-10}$ at 95% C.L. for a mass of $58\,\mu$eV (i. e. 14 GHz). This was the first experimental result with an apparatus exploiting the coupling between cosmological axions and electrons.

We use a cylindrical copper cavity with TM110 mode with resonance frequency $f_c \simeq 13.98$ GHz and linewidth $k_c/2\pi \simeq 400$ kHz at liquid helium temperature, measured with a critically coupled antenna. The cavity mode is coupled to a magnetic material. Highest values of spin density n_s together with long relaxation times have been found for YIG (Yttrium Iron Garnet) and GaYIG (Gallium doped YIG). The amplitude of an external magnetic field B_0 determines the Larmor frequency of the electrons. The uniformity of B_0 on all the spheres must be enough to avoid inhomogeneous broadening of the ferromagnetic resonance. To achieve a magnetic field uniformity $\leq 1/Q_h$, where $Q_h \sim 10^4$ is the quality factor of the hybrid mode, we make use of a superconducting NbTi cylindrical magnet equipped with a concentric cylindrical NbTi correction magnet. With $B_0 = 0.5$ T we have $f_L \simeq f_c$ and thus the hybridization of the cavity and Kittel modes. The power supply of the main magnet is a high-precision, high-stability current generator, injecting 15.416 A into the magnet with a precision better than 1 mA, while a stable current generator provides 26.0 A for the correction magnet. A simplified scheme of the cavity, material and magnet setup is represented in the left part of Fig. 1.

The detection electronics consists in an amplification chain which has two inputs, called Input Channel 1 and 2, (IC-1 and IC-2, respectively). Channel 1 measures the signal power, while Channel 2 has calibration and characterization purposes. A cryogenic switch is used to select the desired channel:

IC-1 - The rf power inside the cavity is collected with a dipole antenna whose coupling to the cavity can be changed using an external micro-manipulator, allowing us to switch continuously from sub-critical to over-critical coupling. For optimal measurement conditions, we tune the antenna to critical coupling by doubling the sub-critical linewidth of the selected mode;

IC-2 - A 50 Ω termination R_J, enclosed in a copper block together with a heater resistance, is used as Johnson noise source. The emitted power can be used to calibrate the noise temperature of the system and the total gain.

The detection electronics, as shown in Fig. 1, is divided into a liquid helium temperature part (LTE)

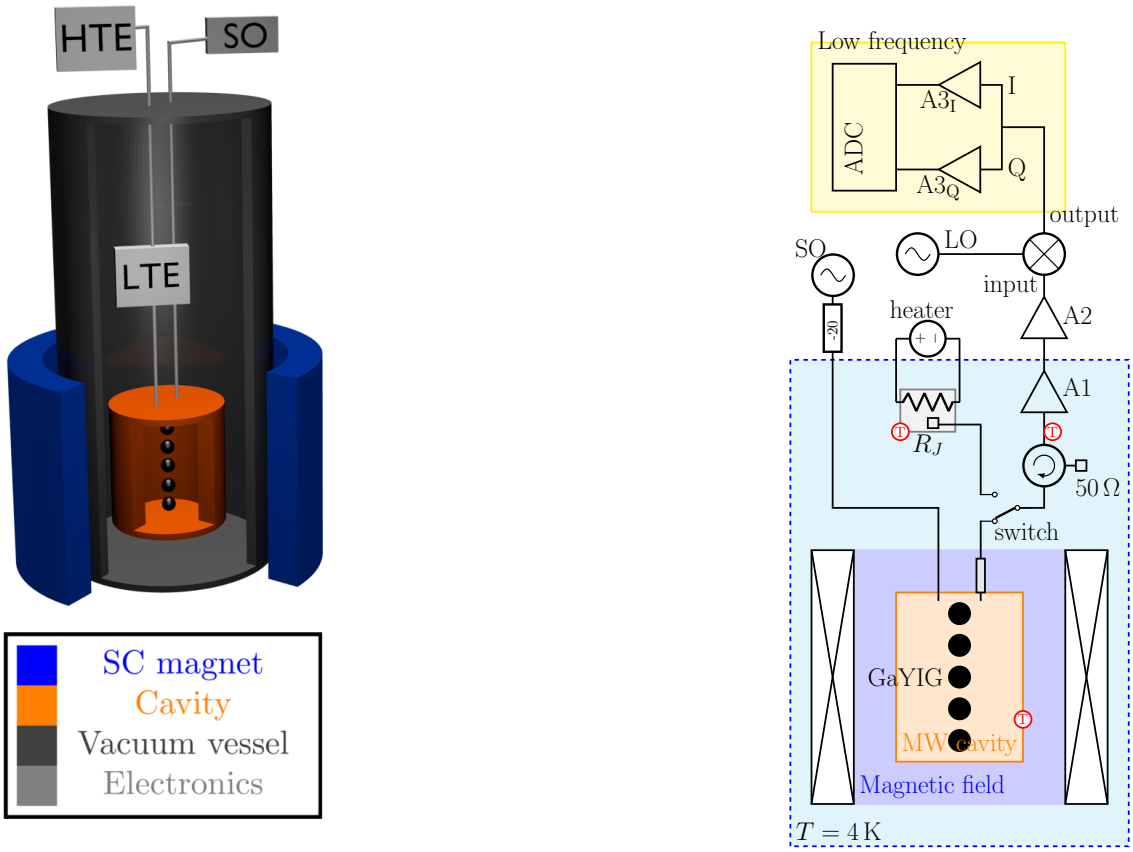

Figure 1: *Left* - Simplified scheme (not to scale) of the experimental apparatus showing the high temperature and low temperature electronics (HTE and LTE) and the source oscillator (SO). *Right* - Electronics layout. From bottom to top, the blue-dashed line encloses the cryogenic part of the apparatus, the crossed rectangles represent the magnet, the orange rectangle is the cavity with black spheres inside standing for the ferrimagnetic material. At the top of the cavity are located the sub-critical antenna (left) and the variably-coupled antenna (right). The sub-critical antenna is connected with a room temperature attenuator and then to the source oscillator SO, while the other antenna is connected to one of the switch inputs. The other input is the 50 Ω resistor R_J, and the gray rectangle is the plate where R_J is placed and that can be heated with a current generator. The output of the switch is connected to an isolator and then to the A1 and A2 amplifiers. The rf coming from A2 is down-converted by mixing it with a local oscillator LO. The two outputs, phase I and quadrature Q, are fed into the low frequency amplifiers $\mathrm{A3}_I$ and $\mathrm{A3}_Q$, and eventually to the ADC. The red T's are thermometers.

and a room temperature part(HTE). The collected power is amplified by a HEMT cryogenic low-noise amplifier (A1) with gain $G_{\mathrm{A1}} \simeq 38\,\mathrm{dB}$. To avoid the back-action noise of the amplifier, a cryogenic isolator with 18 dB of isolation is inserted in the chain. The HTE consists of a room temperature FET amplifier (A2), with $G_{\mathrm{A2}} \simeq 34\,\mathrm{dB}$, followed by an IQ mixer used to down-convert the signal with a local oscillator (LO). The antenna output at the hybrid mode frequency is down-converted in the 0 - 1 MHz band, allowing us to efficiently digitize the signal. The phase and quadrature outputs are fed to two low frequency amplifiers ($\mathrm{A3}_{I,Q}$), with a gain of $G_3 \simeq 50\,\mathrm{dB}$

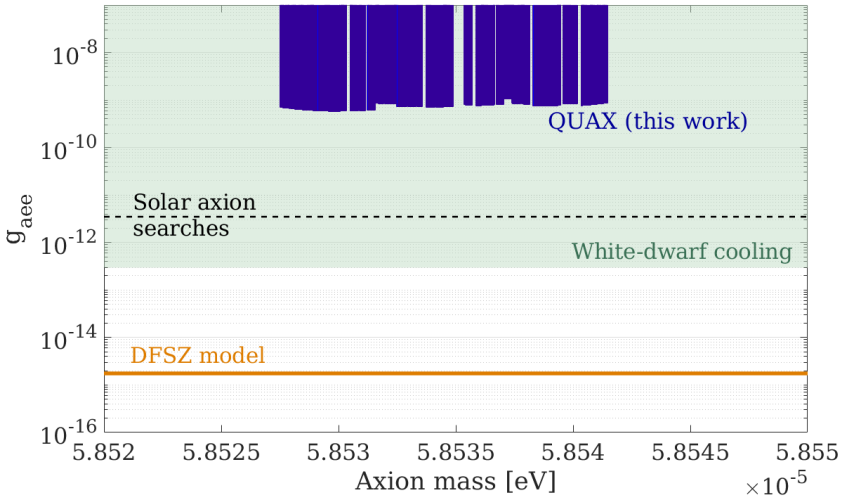

Figure 2: Excluded values of the g_{aee} coupling (blue area) compared to its theoretical prediction for the DFSZ axion model (orange line) and a DM density of $0.45\,\mathrm{GeV/cm^3}$. The green shaded area is excluded by white dwarf cooling, while the black dashed line is the best upper limit obtained with solar axion searches relying on the axio-electric effect.

each, and are acquired by a 16 bit ADC sampling at 2 MHz.

The measured rf power was compatible with the modeled noise for every bin and no statistically significant signal consistent with axions was found. We set an upper limit at the 95% C.L. shown in Fig. 2. The minimum measured value of g_{aee} is 4.9×10^{-10}, corresponding to an equivalent axion field limit of 1.6×10^{-17} T.

2 Microwave losses in a dc magnetic field in super-conducting cavities for axion studies

In order to measure the vanishing signal expected in a haloscope ($P \sim 10^{-23}$W) a high-Q cavity is needed, with $Q \sim 10^6$. Superconducting RF technology can satisfy the requirement of operation in moderate-to-high DC magnetic fields. In a recent paper [2)] we presented an experimental study of the behavior of superconducting cavities in the vortex state. This study has been realized using 14 GHz Cu-NbTi and Cu-NbTiNx film cavities. We measured the magnetic field dependence of the Q-factor and $\Delta\nu/\nu$ where ν is resonant frequency, in the range $B = 0 \div 6$ T at 4.2 K. Also Q versus temperature at fixed B in zero field cooling (ZFC) and field cooling (FC) setups were considered. A comparison was made with Cu and Nb cylindrical bulk cavities. The data for Q vs B were analyzed in terms of the elastic and dissipative motion of flux lines, thus including flux flow and flux pinning.

The RF cavities have been realized with a particular design. Those with the NbTi and NbTiN thin films on Cu bulk are cylindrical (Φ = 26 mm, L=50 mm) hybrid cavities with Cu conical-shaped end-caps to reduce the current dissipation at interfaces. The films have been realized on the cylindrical central region of two specular Cu semi-cell with planar sputtering magnetron (Fig. 3). The film thickness is around 3 to 4 μm, chosen to be in the bulk regime even considering the mixed state penetration depth. Nb and Cu bulk cavities with a cylindrical geometry have been realized for comparison. To characterize the cavities, a RF versatile cryogenic insert for a thermally

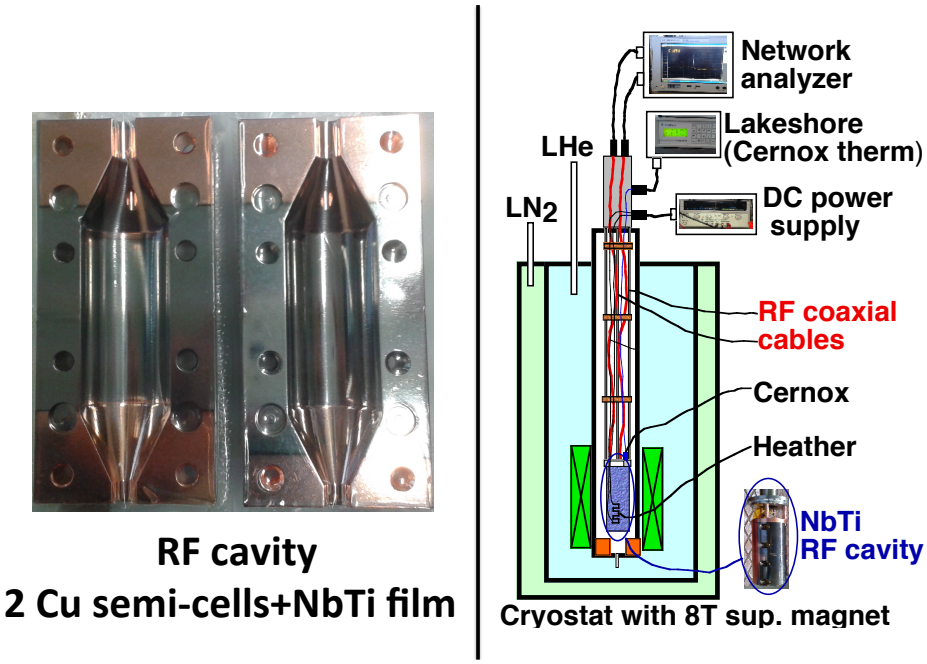

Figure 3: *Left* - Superconducting Hybrid NbTi cavity with Cu conical-shaped end-caps. Two specular Cu semi-cell with NbTi film are shown. *Right* - Cryostat set-up for RF measurement.

controlled gas-flow cryostat, with a superconducting magnet operated up to 8 T, has been made. The RF insert is composed of three different parts: (i) a Connector Head, where two coaxial cables acting as antennas are passed through SMA connectors. The antennas can be inserted with a 10 μm depth resolution into the cavity with two micrometers and are externally connected to a Vector Network Analyzer (Agilent 5071C). The latter is used at very low RF power to measure the loaded quality factor Q_L and cavity frequency, while the unloaded Q_0 was derived from a fit to the waveforms of the coupling coefficients S_{11} and S_{12} as a function of frequency; (ii) a Support tube which connects the bottom of the Connector Head with the RF cavity. An Al vessel isolates the antennas-cavity system from direct contact with flowing liquid helium; (iii) a Sample Holder, which consists of the cavity itself on which a heater and thermometers are mounted. Q_L quality factors were measured as a function of the applied magnetic field B in the range between $0 \div 6$ T at 4.2 K temperature, and versus the temperature with fixed B values. All the measurements have been performed with zero-field-cooling (ZFC) and partial field-cooling (FC) set-ups. The unloaded quality factors Q_0 measured for different resonant cavities are shown in Fig. 4 together with the product $Q_0 B^2$ that appears in the expression of the expected power generated by axions inside the cavity. The comparison of quality factors of NbTi and copper cavities shows a factor 5 gain with 5 T applied magnetic field.

We extracted the complex surface impedance from the variation of the quality factor Q_0 and resonance frequency ν_c as a function of the applied magnetic field B. Infact, according to the standard cavity perturbation theory:

$$\Delta Z_s = G\left(\frac{1}{Q_0(B)} - \frac{1}{Q_0(0)}\right) - i2G\left(\frac{\nu_c(B) - \nu_c(0)}{\nu_c(0)}\right) \quad (1)$$

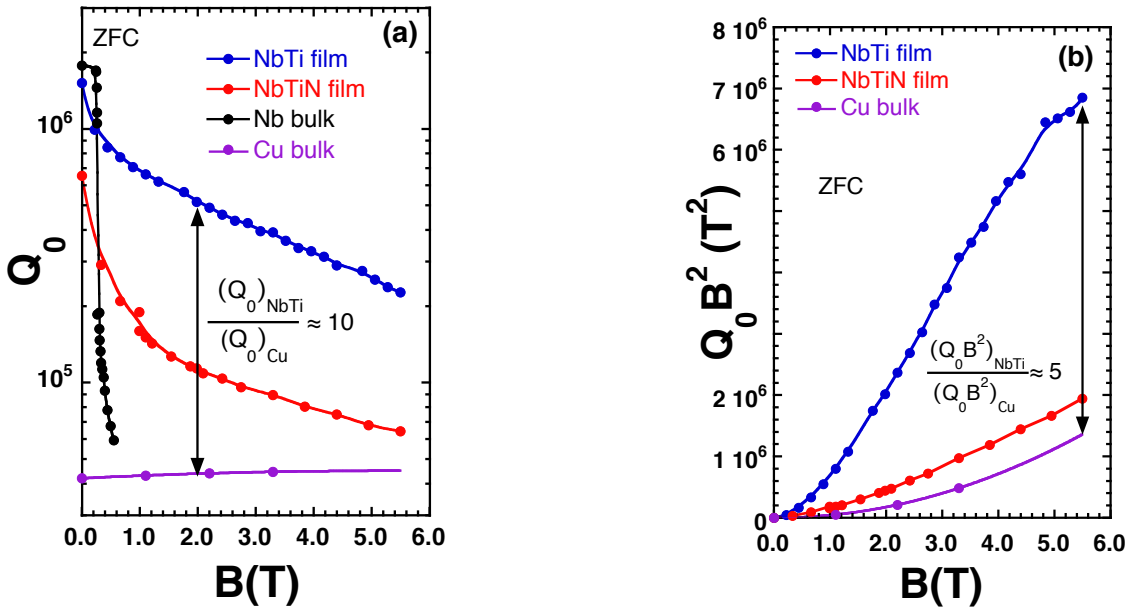

Figure 4: *Left* - Q_0 vs B (figure of merit in the axion-spin electron conversion). *Right* - $Q_0 B^2$ vs B (figure of merit in the direct axion-photon conversion), both at T=4.2 K and 14.46 GHz.

were G is the cavity geometrical factor. These results were interpreted according to the Gittleman and Rosenblum model (GR) [3, 4]. In Fig. 5 we show the results of our analysis for both NbTi and NbTiN cavities. Using the Z_s expression from the GR model, taking into account the vortex motion resistivity, we fit the experimental data. A good agreement between data and theoretical model is observed in figure 5. From the fit procedure we extract the depinning frequency ν_p. This frequency sets the value of applied RF frequency above which the vortices start dissipating and the quality factor of the cavity deteriorates. For NbTi we observed $\nu_p = 45$ GHz, meaning that this material is preferable to copper at least up to this frequency value, e.g. for axion searches up to mass $m_a = 150$ μeV.

3 List of Conference Talks by LNF Authors in Year 2018

Include a list of conference talks by LNF authors.

1. D. Di Gioacchino,"Microwave losses in dc magnetic field with superconducting cavities for axion studies", Applied Superconductivity Conference Seattle 2018, October 28 November 2.

2. C. Gatti, "Status report of the QUAX R&D activity", 14th AxionWIMP conference (Patras workshop) 17-22 June 2018 DESY in Hamburg.

4 Publications

- "Operation of a ferromagnetic axion haloscope at $m_a = 58\mu$eV," Eur. Phys. J. C (2018) 78:703 [1].

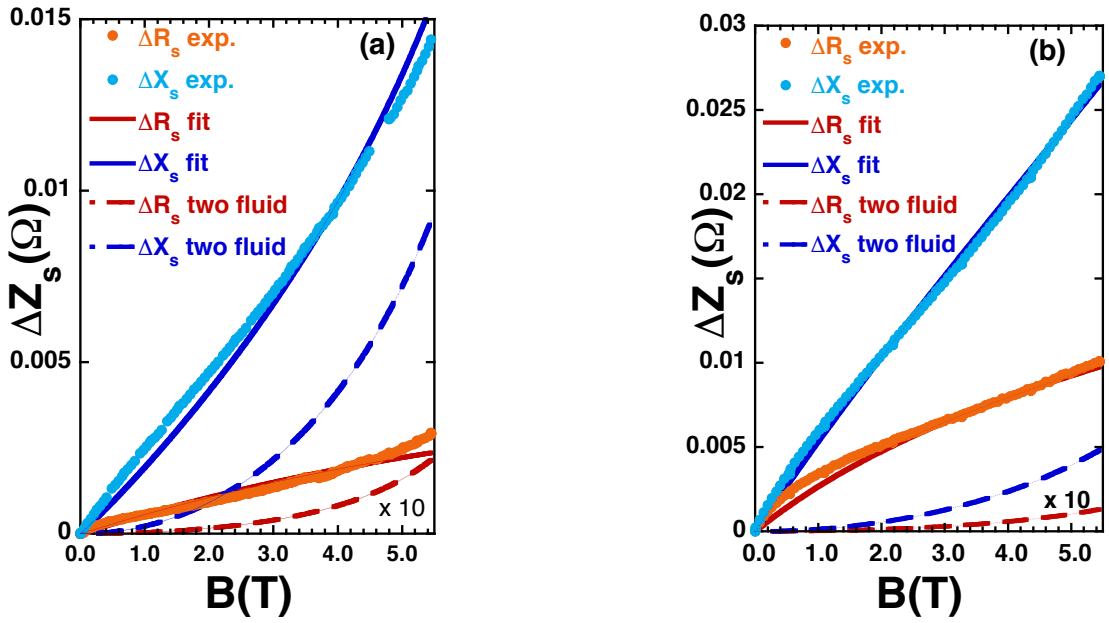

Figure 5: ΔZ_s vs B at ∼4.2 K for the NbTi (a) and NbTiN (b) cavity, mode TM110. Experimental data (full dots), two-fluid only numerical model (dashed lines), two-fluid plus vortex motion numerical model (GR) (continuous line).

- "Microwave losses in a dc magnetic field in superconducting cavities for axion studies," IEEE Trans. Appl. Sup. **29**, no. 5, (2019) [2)].

References

1. N. Crescini et al.,"Operation of a ferromagnetic axion haloscope at $m_a = 58\mu$eV," Eur. Phys. J. C (2018) 78:703.
2. D. Di Gioacchino et al.,"Microwave losses in a dc magnetic field in superconducting cavities for axion studies," IEEE Trans. Appl. Sup. **29**, no. 5, (2019).
3. J. I. Gittleman and B. Rosenblum,Radio-Frequency Resistance in the Mixed State for Subcritical Currents Physical Review Letters, vol.16, no.17, pp.734-736, Apr. 1966.
4. N. Pompeo and E. Silva, Reliable determination of vortex parameters from measurements of the microwave complex resistivity, Phys. Rev. B, vol. 78, no. 9, p. 094503, Sep. 2008.